Schweizerische Eidgenossenschaft
Confédération suisse
Confederazione Svizzera
Confederaziun svizra

Eidgenössisches Departement für
Umwelt, Verkehr, Energie und Kommunikation UVEK

Bundesamt für Energie BFE

PROJEKTTITEL: ENTWICKLUNG UND VALIDIERUNG VERBESSERTER TEILMODELLE FÜR TRANSIENTE SPRAYS MIT VERBRENNUNG

Schlussbericht 2006

Autor und Koautoren	Dipl.Ing. Ourania-Nektaria Margari, Prof. K. Boulouchos
beauftragte Institution	Laboratorium für Aerothermochemie und Verbrennungssysteme
Adresse	Sonneggstrasse 3, ETH Zentrum CH-8092 Zurich
Telefon, E-mail, Internetadresse	044 632 77 85, margari@lav.mavt.ethz.ch, www.lav.ethz.ch
BFE Projekt-/Vertrag-Nummer	47495/87575
BFE-Projektleiter	Dr. A. Hintermann
Dauer des Projekts (von – bis)	1. Oktober 2002-31. Dezember 2006
Datum	11.12.2006

ZUSAMMENFASSUNG

Diese Arbeit beschäftigt sich mit einer detaillierten Analyse von Emissionswerten für Direkteinspritzung bei Dieselmotoren. Beim Einsatz berührungsloser optischer Messverfahren wird eine Analyse der Verbrennungsprozesse benötigt, um ein Verständnis für die Russbildung und der dabei einhergehenden Oxidationsprozesse zu erlangen. Um dieses Ziel zu erreichen, wird eine experimentelle Untersuchung in einer Hochtemperatur- und Hochdruckzelle am LAV der ETH Zürich durchgeführt. Zur Untersuchung der Russbildung bei transienten Dieselstrahlen wurden die beiden laseroptischen Verfahren Mehrwellenlängenpyrometrie und „back diffused laser technique" (BDL) simultan angewandt. Eine Analyse wurde durchgeführt, basierend auf dem aufgezeichneten Drucksignal und dem detektierten Flammenlicht, zur Identifizierung des Zündverzugs, der Dauer der Vormischverbrennung, des Einsatzes der diffusiven Verbrennung und der gesamten Brenndauer. Zum Einsatz kommen ein Referenzdieselkraftstoff, sowie unterschiedliche Zumischungen von Butylal (sauerstoffhaltig) und Wasser-Dieselemulsionen, wobei der Einspritzdruck variiert wird und sowohl der eingespritzte Massenstrom, die Zelltemperatur als auch der Zelldruck vor dem Einspritzen konstant gehalten werden. Die Bildung von „Particulate Matter" (PM) Emissions wird unter gleichen Bedingungen untersucht.

Ein Vergleich der beiden Messverfahren zeigt auf, dass obwohl die KL-Faktoren (ein Mass für die Russkonzentration) wie sie basierend auf dem Pyrometerverfahren berechnet werden, höher sind als im Falle des BDL Verfahrens, der Trend der mittleren KL-Faktoren derer zeitlichen Integration nach dem Einspritzen für beide Verfahren vergleichbar sind. Darüber hinaus wurde der Einfluss des Einspritzdruckes untersucht, wobei die eingespritzte Kraftstoffmasse konstant gehalten wurde. Es zeigt sich, dass eine Änderung des Einspritzdruckes von 500bar bis 900bar einen Abfall der mittleren Temperatur und des volumetrischen Anteiles der Russwolke bewirkt. Von 900bar bis 1300bar bleibt sowohl die mittlere Temperatur als auch die Wärmeabgabe konstant, während das Maximum des volumetrischen Russanteiles zu höheren Werten tendiert jedoch unter höheren Oxidationsraten. Zuallerletzt wurde der Einfluss der Brennstoffeigenschaften untersucht unter Einsatz folgender Brennstoffzusammensetzungen: Diesel, zwei Mischungen (25% und 50% nach Masse) mit sauerstoffangereichertem Dieselzusatz (Butylal) und zwei Wasser-Diesel Emulsionen (13% und 25% nach Masse). Pyrometerergebnisse zeigen auf, dass die mittlere Temperatur der Russwolke als eine Funktion des Brennstoffgemisches abfällt mit folgender Reihenfolge: Diesel, Butylal-Diesel 25%, Butylal-Diesel 50%, Wasser-Diesel Emulsion 13% und 25%. Sowohl der KL-Faktor als auch dessen zeitliche Integration zeigen den gleichen Trend auf. Butylal beinhaltet Sauerstoff und weist im Vergleich zum Diesel eine höhere Cetanzahl (CN) auf. Die höhere Konzentration von Sauerstoff im Gemisch ermöglicht eine bessere Russoxidation. Emulsionen beinhalten Wasser, dass die Flammtemperatur herabsetzt und den Zündverzug vergrössert. Der Kühlungseffekt des verdampfenden Wassers hängt vom eingespritzten Wasseranteil im Gemisch ab. Die Tröpfchenverdampfung des Wassers bewirkt eine sekundäre Atomisierung und begünstigt damit die Vermischung von Luft und Brennstoff. Die gewonnenen Ergebnisse werden eingesetzt um derzeitige Modellierungen der Verbrennungsvorgänge in Dieselmotoren im Hinblick auf Russbildung und Oxidationsvorgänge zu erweitern. Die im Rahmen dieses Projektes aufgebaute experimentelle Datenbank wird auch internationalen Partnern zur Verfügung gestellt.

Projektziele

One of the main goals of this project is to acquire a large data set for a detailed study of the emission levels that are produced by the direct injection Diesel engines, so that currently available or future simulation models can be validated. In order to meet future emission regulations, both on-road and off-road heavy-duty diesel engines will require minimized cylinder-out emissions and the use of exhaust after treatment technologies. In-cylinder emission control technologies, as e.g. fuel injection system optimization and modification of fuel composition are investigated in detail at our laboratory. A good analysis of the combustion processes will lead to the comprehension of these phenomena and the reduction of the emission levels, without impairing the engine performance and efficiency. In order to achieve this goal an experimental work is performed in *LAV*/ETH in a High temperature-high pressure cell (Figure 1). The advantage of a combustion cell is its ability to simulate a wide range of conditions, including those found in the real Diesel engines.

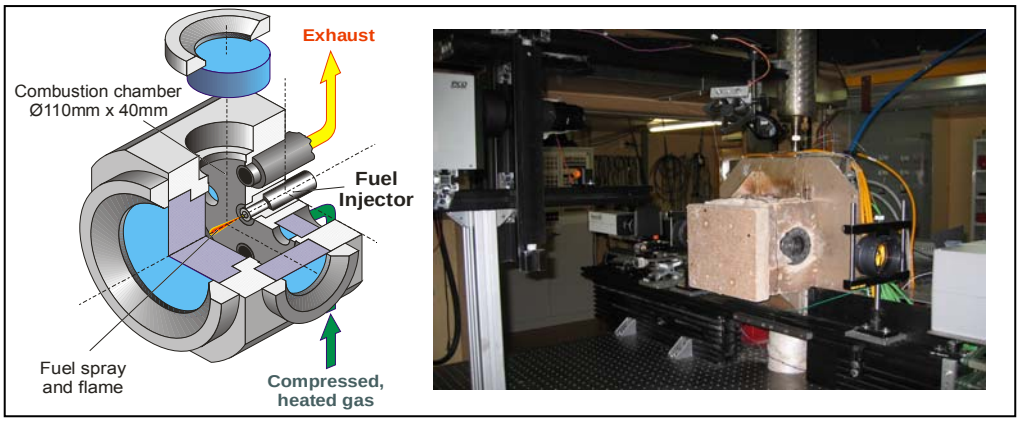

Figure 1: High temperature-high pressure cell

Durchgeführte Arbeiten und erreichte Ergebnisse

The major part of Diesel combustion involves diffusion flames. One of the characteristics of this type of combustion is its high luminosity caused by the thermal radiation of soot particles at high temperatures. Two techniques, the two-color pyrometry and the back diffused laser technique (BDL) will be presented and results will be discussed. Since it is difficult to get enough optical access inside a running Diesel engine the constant volume high-pressure-high-temperature cell (HTDZ) is used. This facility has full optical access and can deliver answers to the basics of soot formation and oxidation during the combustion process.

Measurement techniques

Back Diffused Laser (BDL) Technique

The experimental set-up of the BDL apparatus is shown in Figure 2. A frequency-doubled Nd:YAG laser, wavelength 532nm, is used as the laser light source. A pair of spherical lenses is used to diffuse the laser beam onto a white screen. A 35mm diameter objective lens collects the transmitted light through a narrow band pass filter (band pass of 532nm and FWHM=10nm) onto the 1280×1024 pixel screen of 12 bit CCD camera. The camera's exposure time is 0.5μs and the pulse duration is 8ns. During the measurements, two images are recorded. The first image is obtained in the absence of spray combustion to provide a measure of the initial light intensity I_0. A second image is obtained during combustion to record the attenuation light intensity I. The use of the bandpass filter eliminates the luminosity of the flame, and images only the liquid droplets, such as unevaporated fuel, and the soot particles within the flame's shadows.

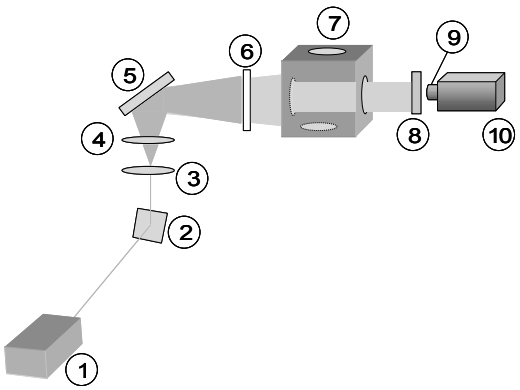

Figure 2: Schematic of the BDL setup

[1]	Nd:YAG laser	[6]	White screen
[2]	High energy mirror	[7]	High-temperature high-pressure cell
[3]	First lens to diffuse the laser beam	[8]	Line band pass filter
[4]	Second lens to diffuse the laser beam	[9]	Objective
[5]	High energy mirror	[10]	CCD camera

Pyrometer

A schematic diagram of the pyrometer set-up is shown in Figure 3. The light emitted from the flame enters the optical set-up through the zoom objective lens. The captured light is converged by the lens, and then collimated by a *f*=127mm lens, lens 1. A dichroic beam splitter is used to split the collimated beam into two parts. Since the reflected portion of this beam is subsequently passed through a 740nm bandpass filter of 4nm full width at half maximum (FWHM), this beam splitter is also referred to the 'hot' mirror. The transmitted portion of the collimated beam is passed through a 640nm bandpass filter of FWHM 2nm, and then, with the aid of the 'cold' mirror - the second dichroic beam splitter - is combined with the 740nm beam. A pair of adjustable, precision mirrors that are located between the beam splitters and bandpass filters are employed to ensure that the images of both flames - from the 640nm and 740nm beams - are projected through a second lens onto the image plane of an intensive CCD camera. The HeNe laser is used in the alignment of the optical components.

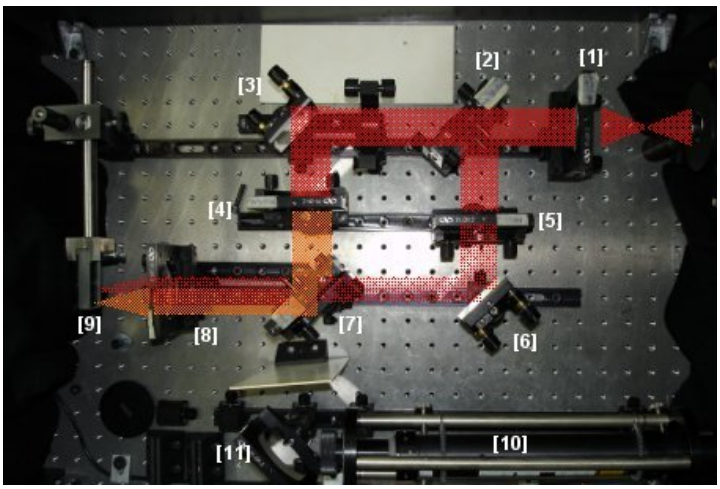

Figure 3: Optical setup two-colour pyrometry

[1]	First lens (f = 127 mm)	[7]	Dichroic beam splitter ("cold mirror")
[2]	Dichroic beam splitter ("hot mirror")	[8]	Second lens (f = 127 mm)
[3]	Adjustable mirror	[9]	Optical prism
[4]	Band-pass-filter (640 nm)	[10]	HeNe-laser
[5]	Band-pass-filter (740 nm)	[11]	Fix mirror
[6]	Adjustable mirror		

Results

Comparison BDL-Pyrometry

In Figure 4 the spatial comparison between the mean KL-factor (over 20 records) calculated from pyrometry and back diffused laser technique (BDL) is presented correspondingly, for diesel fuel, at 500bar of injection pressure for all time steps recorded. The black contour plots indicate the pyrometer results, while the color contours plots specify the BDL outcome. Both plots are geometrically calibrated and merged each other (Figure 4). It is observed that the soot cloud captured by pyrometer is larger compared to the soot cloud recorded by BDL.

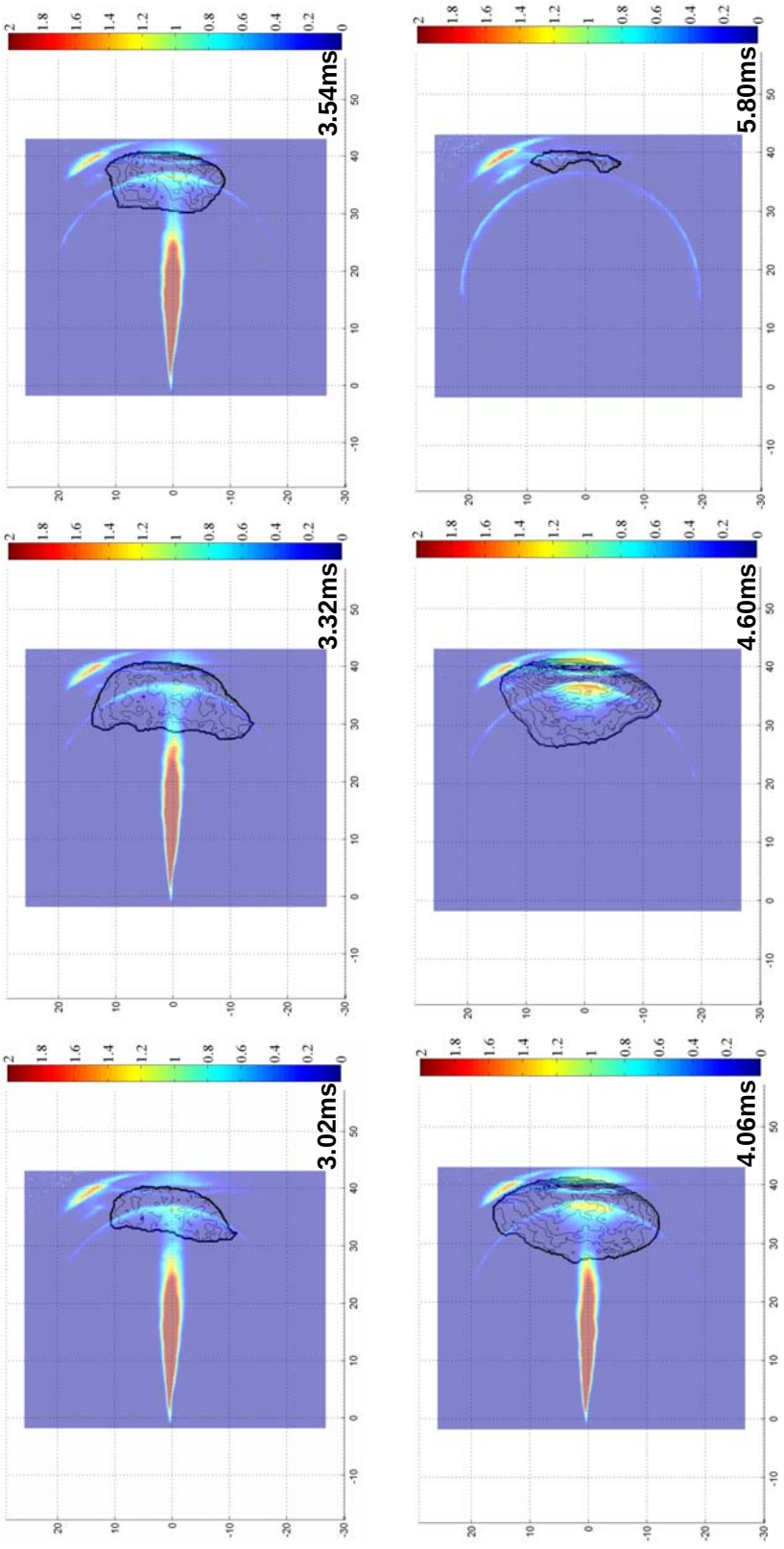

Figure 4: *Spatial comparison between pyrometry (black contour plots) and BDL technique (colored contour plots), using Diesel fuel at the operation conditions: p_{cell}=60bar, T_{cell}=790K, p_{inj}=500bar and t_{inj}=4.25ms.*

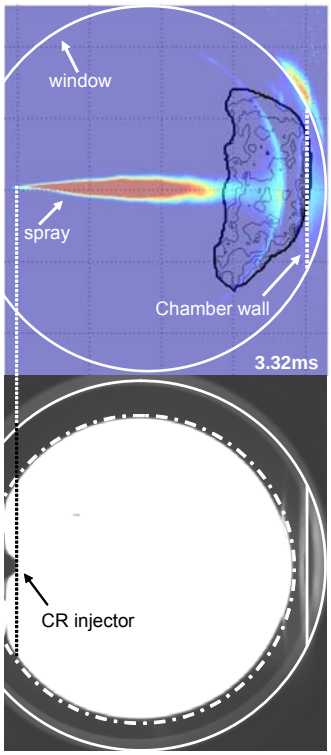

(a)

(b)

Figure 5: *(a)Characteristics of the BDL image and (b) the volume of the combustion chamber and the area (between the dashed and the solid cycle) where the extinction method cannot be applied. This is the I_0 used for the BDL calculation*

Observing *Figure 5(b)*, where the volume of the chamber is presented as the I_0 (for BDL technique) it can be seen that the extinction of the laser light intensity does not take place in the whole combustion chamber. The area between the dashed and the solid (the window border) circle, indicate the region in the chamber where it is not possible to get results from the BDL. Based on this observation, the part of the soot cloud, calculated with pyrometer, located in this area is cut-out (only for the comparison). In this case the spatial evolution of the soot cloud for both techniques is presented in Figure 6.

The mean KL-factor of the soot cloud recorded with both techniques is calculated in two ways: First, it is averaged and integrated on the total soot cloud. Second, the same calculation is done based on the common area that the soot clouds occupy (masked area). In both cases, the mean KL-factor (measured with BDL) was evaluated neglecting the fuel spray and additional reflections (*Figure 5(a)*).

Figure 7*(a)* shows the mean KL-factor and its integral for diesel fuel at 500bar over the time after start ASOI. The square symbols indicate the pyrometer results and the triangles the BDL outcome. The empty and filled symbols correspond to the first and the second case, respectively. In both cases, the comparison shows similar trends of soot formation and oxidation process. More specifically, pyrometer measurements have higher values of mean KL-factor compared to the BDL technique. The mean KL values calculated with BDL are 45% and 60% lower compared to pyrometer results for both cases respectively. The integral of the KL-factor for both cases, measured by both techniques, follow, qualitatively, similar trend, but indicates that BDL gives lower values by 70 and 87% when compared to pyrometer. It would be expected that the integral of the KL-factor measured with pyrometer would give lower values than with BDL, but this does not happen. The main difference between these two measurement methods is that pyrometer captures only the 'hot' soot, since radiation intensity scales with the forth power of temperature, whereas BDL measures the complete soot range within the measuring volume. BDL technique works as the shadowgraphy, i.e. the shadow of the particulate matter and the spray liquid phase is recorded. This means that except the 'hot' soot, captured by pyrometer, the 'cold' soot is as well recorded. Moreover, because of the variation of soot opacity with wavelength ($KL = \frac{\kappa L}{\lambda^{\alpha}}$), the KL-factor should be higher by 40% at 532nm when compared to the mean of 640 and 740nm.

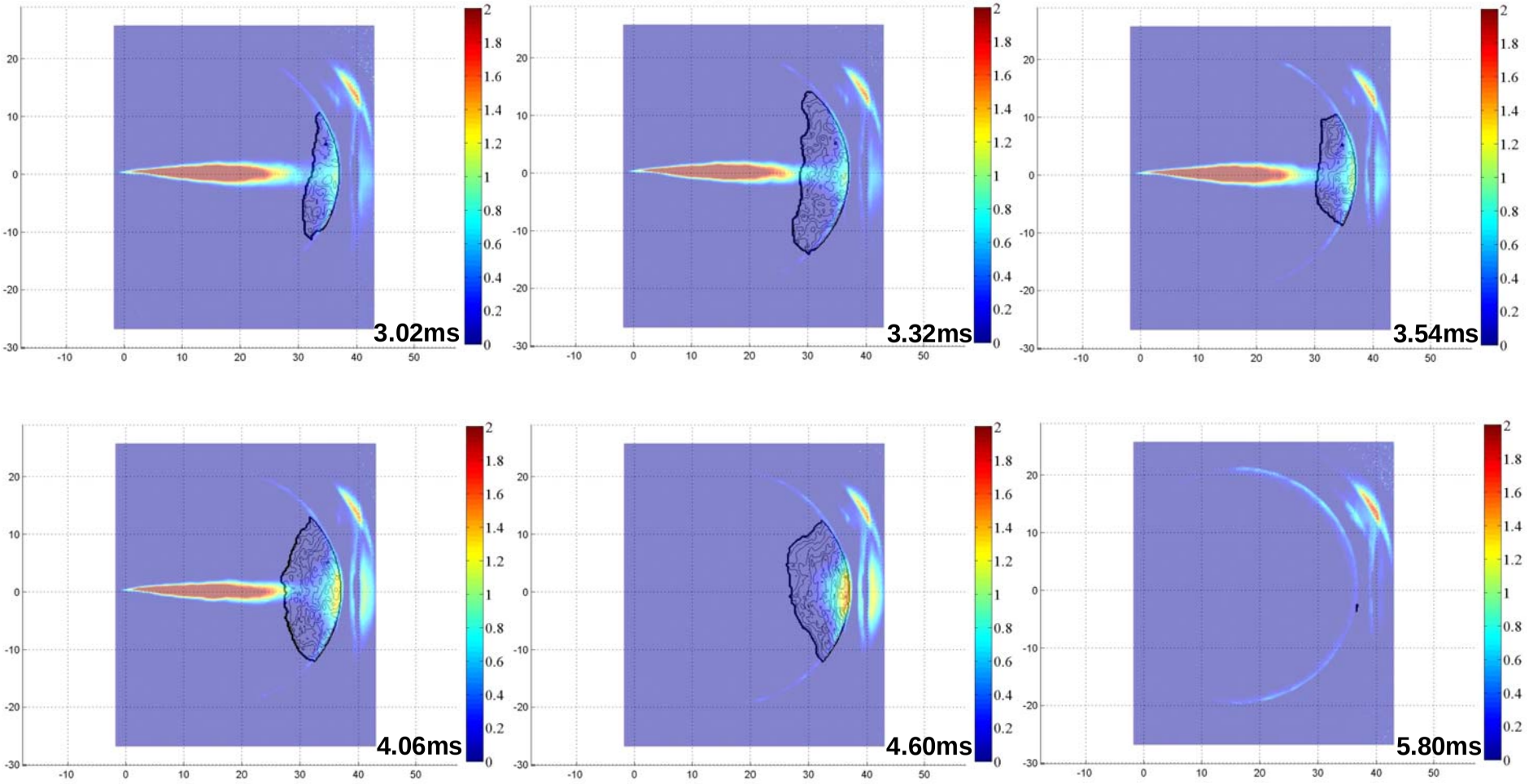

Figure 6: *Spatial comparison between the masked pyrometry (black contour plots) and BDL technique (color contour plots), using Diesel fuel at the operation conditions: p_{cell}=60bar, T_{cell}=790K, p_{inj}=500bar and t_{inj}=4.25ms.*

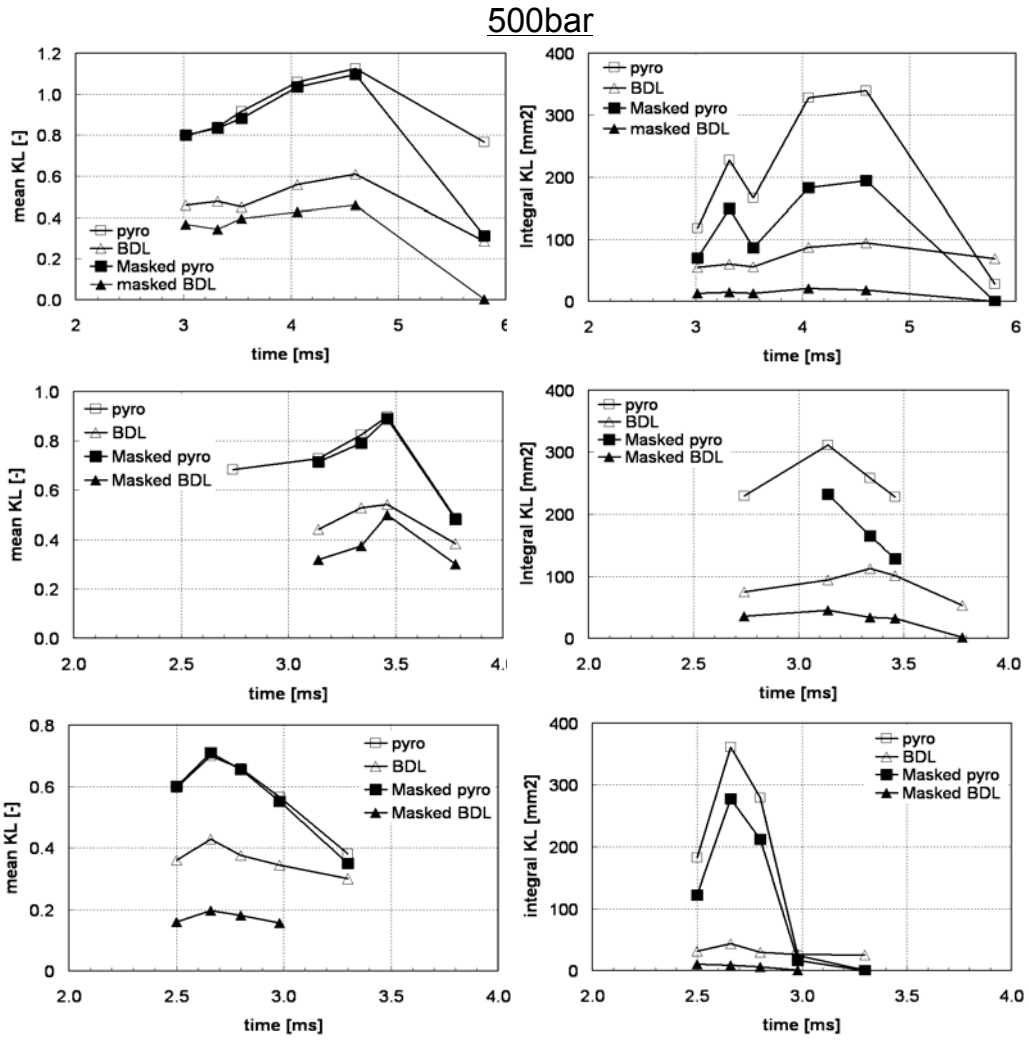

Figure 7: *The mean KL-factor and its integral measured with pyrometry and BDL technique for two cases: the total soot cloud and the masked where the soot cloud coexists in both measurenmnts at (a) 500bar, (b) 900bar and (c) 1300bar, using diesel at operation conditions:* p_{cell}*=60bar,* T_{cell}*=790K,* p_{inj}*=500bar and* t_{inj}*=4.25ms.*

The distribution of the values of KL-factor over the soot cloud is presented for the total amount of soot (first case) and for the masked case for both techniques in Figure 8. The left column presents the histograms of the KL-factor, taking into account the whole soot cloud (first case), while the right column shows the same results for the region of interest of the soot cloud (second case) at different trigger times ASOI. In both cases it is observed that the pyrometer sensitivity is very weak for KL values lower than 0.4 (at 3.32ms ASOI, Figure 8). At the same time, the BDL sensitivity to KL values, higher than 1.2, becomes very low too (at 4.06ms ASOI, Figure 8). Looking at the results of the second case (right column at Figure 8), it is seen that the soot cloud calculated by BDL technique occupies much smaller area than the one calculated by pyrometry. This could be because of the weak laser extinction. Pickett et. al. [8] has mentioned that the extinction increases as the number of primary particles in a soot aggregate or the primary particle size increases. Based on this argument, an explanation to the present measurements might be that the soot particles are very small to be captured by BDL technique. The band pass filter used in BDL measurements could also have an influence in the extinction signal. It is very broad (532nm with ±10nm of FWHF) to eliminate the flame luminosity. When measurements with BDL are performed at trigger time smaller than the end of the injection, the non-vaporized liquid phase of the injected fuel and the produced particulate matter in the flame cannot be unambiguously distinguished (Figure 4 and Figure 6). This means that until the moment when the injection finishes, it is difficult to identify the regions where the liquid phase and soot particles may coexist (or not).

The comparison between the pyrometry and the BDL technique has shown that the results follow the same trend, but quantitatively the KL values are very different, with 70% lower the KL values measured with BDL technique. The same behaviour is observed even if the injection pressure increases to 900 and 1300bar (Figure 7). The use of different fuel shows similar results too. For this reason, the rest of the dis-

cussion is based on the pyrometer results since they provide the same range of values of KL-factor as in the literature.

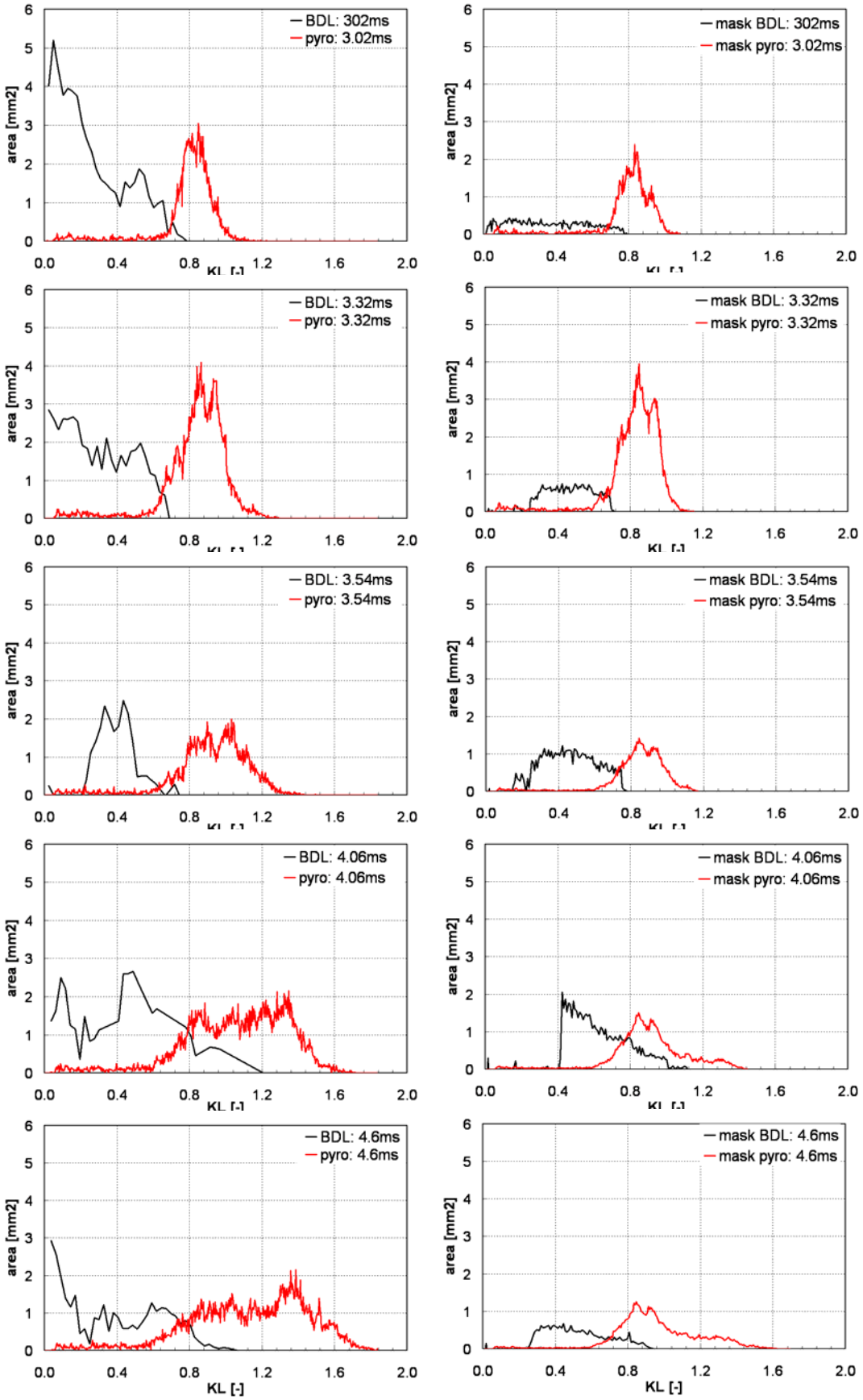

Figure 8: *Comparison of the KL-factor distribution calculated with pyrometer and BDL technique for two cases: total amount of soot (left column) and masked where the soot cloud coexists in both techniques using diesel fuel, at operation conditions: p_{cell}=60bar, T_{cell}=790K, p_{inj}=500bar and t_{inj}=4.25ms.*

Influence of Injection Pressure on the Emissions

Pyrometer results are presented for the three different cases A, B, C (Table 1,Figure 9) in direct comparison to each other.

Fuel	T_{cell} [K]	P_{cell} [bar]	P_{inj} [bar]	m_{inj} [mg]	t_{inj} [ms]
Diesel	790	60	A: 500	17.4	4.25
			B: 900		3.00
			C: 1300		2.50

Table 1: Measurements Matrix

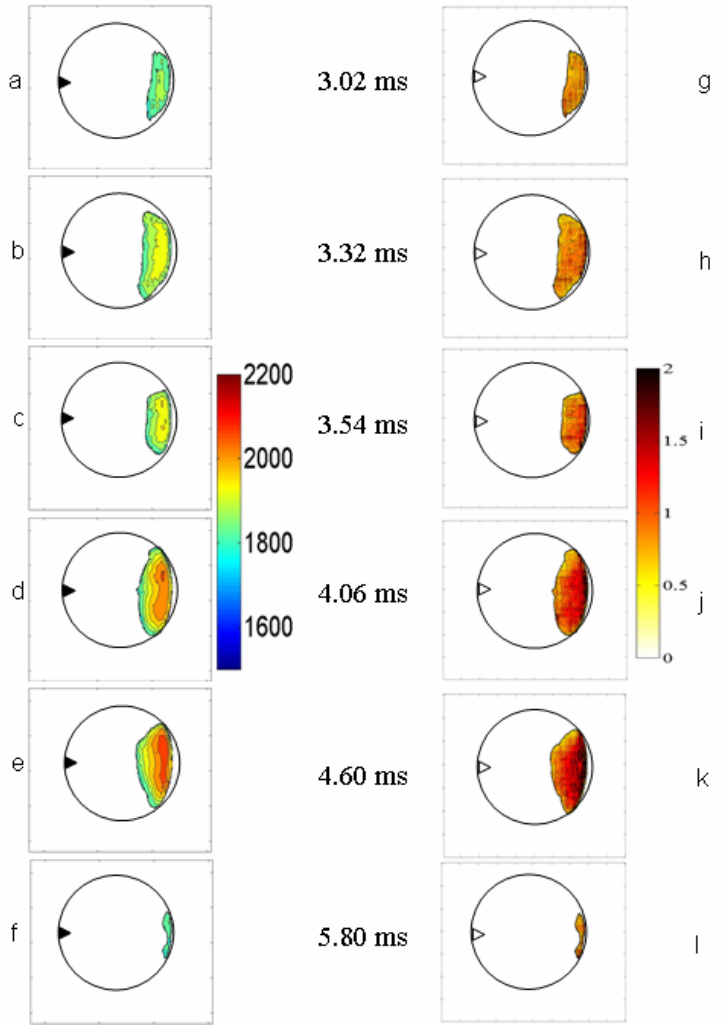

Figure 9: The evolution of flame temperature (left column) and KL-factor (right column), measured with pyrometry, using diesel fuel at case A: p_{cell}=60bar, T_{cell}=790K, p_{inj}=500bar and t_{inj}=4.25ms

First, the temporal and spatial evolution of temperature and the KL-factor of the soot cloud are described in Figure 10 based on the T-KL histograms. The results are based on the average sequence recorded by pyrometry (Figure 9). These histograms show the spatial distribution of the soot temperature and KL-factor over the whole cross section of the soot cloud. In all cases, the gradual process of soot temperature and KL-factor over time after start of injection is observed. In the first case, where the injection pressure is equal to 500bar, the temperature and the KL-factor increase from 3.02ms to 3.32ms; at 3.54ms the values remain almost constant, while at 4.06 to 4.6ms the soot temperature and the KL-factor increase farther. At the end, at 5.8ms after the start of the injection, the temperature and the KL-factor decrease.

Moreover, it is shown that an increase to the soot temperature corresponds to KL-factor increase. Similar behavior is observed to the soot temperature and KL-factor evolution, increasing the injection pressure to 900 and 1300bar.

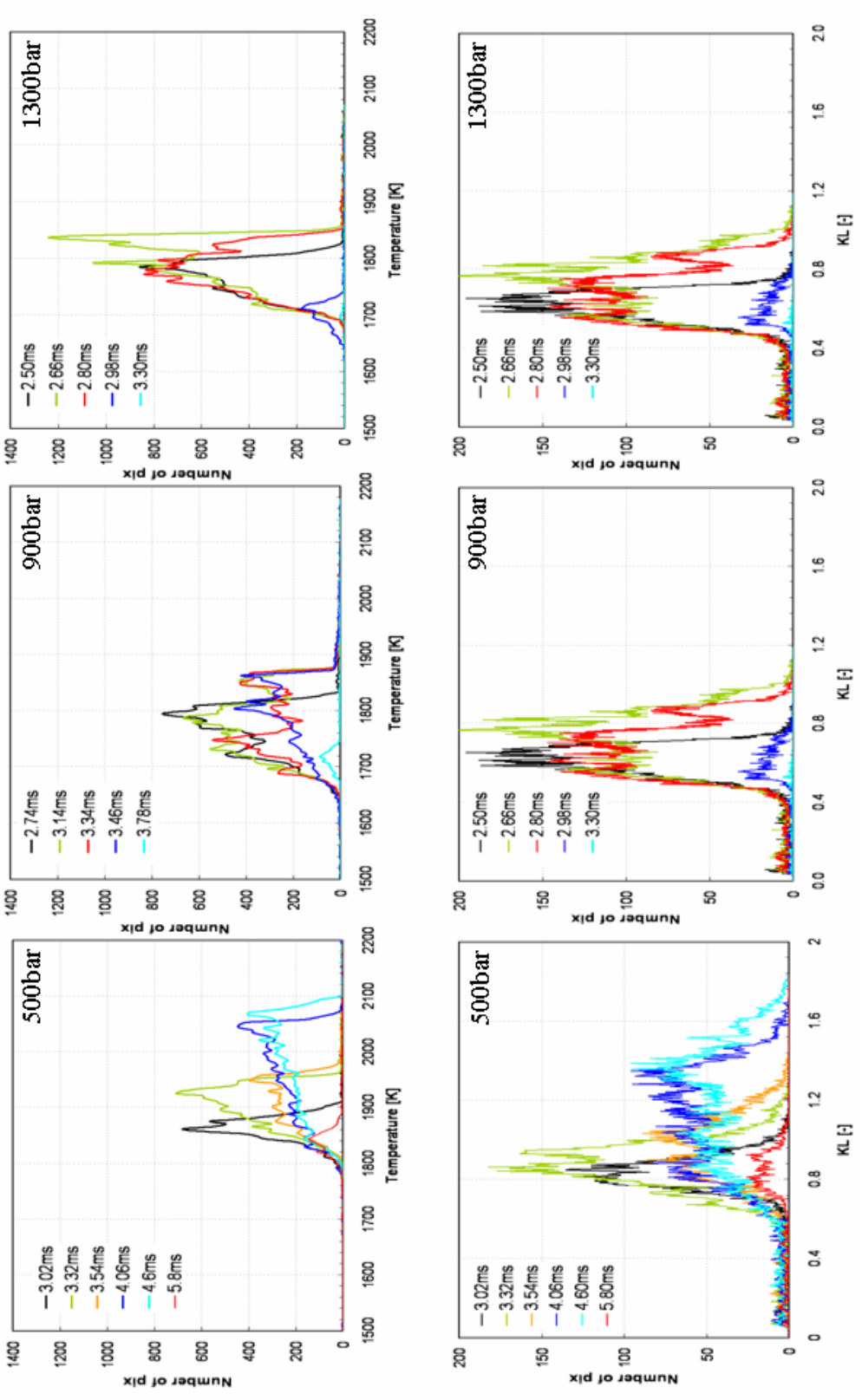

Figure 10: Temporal and spatial evolution of temperature and KL-factor shown by their histograms at three injection pressures, 500, 900 and 1300bar usina baseline diesel fuel

Comparison between the temperature histograms at different injection pressures shows that increasing the injection pressure the temperature decreases. Similar behavior is observed for the KL-factor too. At this point, the spatial correlation between soot temperature and KL-factor is evaluated. The correlation coefficient *r* is defined as:

$$r = \frac{\frac{\sum (T - T_i) \cdot (KL - KL_i)}{N}}{\sqrt{\frac{\sum (T - T_i)^2}{N}} \cdot \sqrt{\frac{\sum (KL - KL_i)^2}{N}}} \quad (1)$$

where N is the number of images (equal to 20), T_i and KL_i the instantaneous temperature and KL-factor. In Figure 11 the correlation coefficient for diesel fuel at three different injection pressures (500/900/1300bar) is presented. The dark red color is equivalent to r=1, which means that between the temperature and KL-factor there is a perfect positive correlation, i.e. they co-vary. When r=-1 (dark blue) there is a perfect negative correlation between T and KL, i.e. they vary in opposite ways. Values between -1 to 1 mean no correlation between T and KL. The first consideration is that the correlation coefficient over time is similar for all cases. Its value lays mainly in the range between 0.8 and 1, meaning that at each time, an increase to the temperature is followed by an increase to the KL-factor. Only in the case A, at injection pressure 500bar, there are regions where the correlation coefficient gets values close to 0, denoting that the soot temperature and the Kl-factor are uncorrelated. These areas are close to the chamber wall, which has lower temperature compared to the soot cloud temperature. In this case the heat transfer between the soot cloud and the wall leads to reduction of the flame temperature. Therefore, not enough soot oxidation takes place; resulting to high values of KL-factor. Increasing the injection pressure this phenomenon is not observed any more, as shown in the Figure 11.

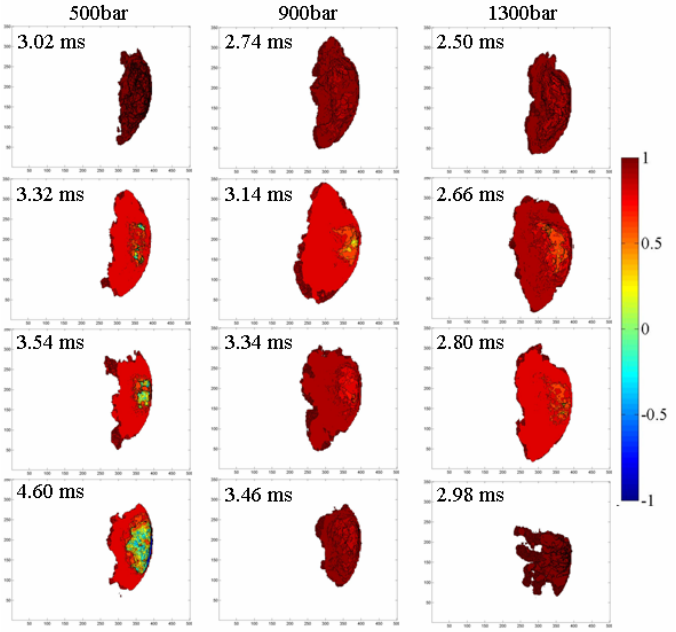

Figure 11: Correlation coefficient between soot temperature and KL-factor for diesel fuel, at 500/900/1300bar injection pressure.

In addition, the mean temperature of soot that corresponds to the ''radiation'' temperature was calculated. Mean temperature is the average temperature over the soot cloud. In Figure 12 the mean ''radiation'' temperature is presented versus the time after the start of injection (ASOI). It is observed that with the increase of the injection pressure the flame temperature drops, i.e. at 500bar the maximum temperature is 1975K, while at 900bar and 1300bar it decreases to 1800K, corresponding to a decrease of 8.8%. However, with further increase of the injection pressure, from 900bar (case B) to 1300bar (case C), the value of the maximum flame temperature does not change significantly, as the ROHR does not differ considerably (Figure 13). Apparently in this case, the combustion mechanism does not change substantially, and thus there is no pressure influence to the flame temperature, injecting constant fuel mass. The decrease of the flame temperature denotes possible reduction of the NO_x emissions. Moreover, in all cases the maximum temperature appears after the end of the fuel injection.

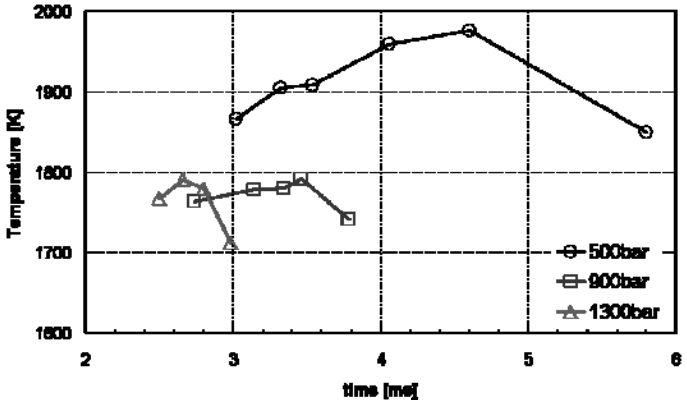

Figure 12: The mean flame temperature versus the time after the start of injection (calculated by pyrometer) at 500bar, 900bar, 1300bar, keeping the injected diesel fuel mass constant

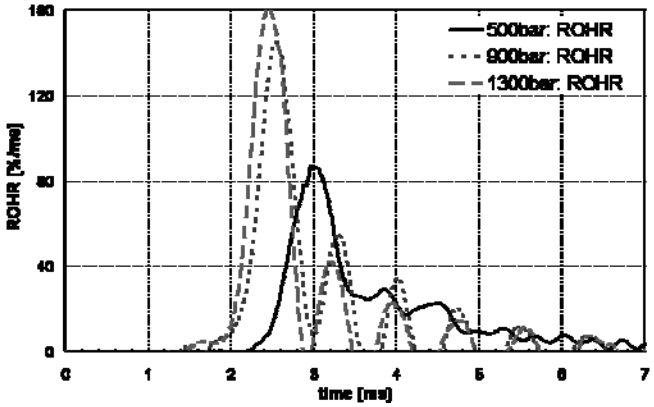

Figure 13: Rate of heat release at different injection pressures: 500bar, 900bar, 1300bar, using diesel fuel and keeping the injected fuel mass constant

In Figure 14 the spatially averaged values of the KL-factor, which correspond to the averaged value of the flame cross section, over time ASOI are shown for different injection pressures. It is observed that the mean KL-factor decreases with the increase of the injection pressure, while the soot formation process starts earlier. When the injection pressure increases, the injection rate raises, thus larger amount of fuel will be undergoing pyrolysis. The spread of the spray is larger, the turbulence is higher and the mixing process better, resulting to stronger oxygen entrainment.

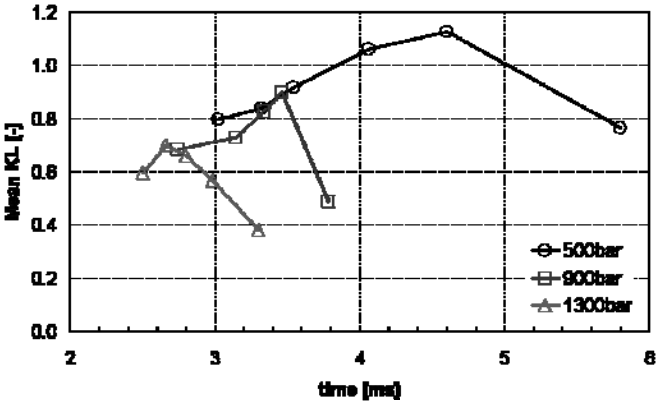

Figure 14: The mean values of KL-factor, using diesel fuel, versus the time after the start of the injection (calculated by pyrometry) at the cross section of the flame, at 500bar, 900bar, 1300bar, keeping the injected fuel mass constant

The integral of the KL-factor, i.e. the sum of the KL-factor over the flame cross section versus the time after the start of injection, is presented *in Figure 15*. This plot represents the total amount of 'hot' soot within the combustion chamber. It is observed that increasing the injection pressure the peak value of the

integral of KL-factor remains almost unchanged. Comparing the results in Figure 14 and Figure 15, it is perceived that the particulate matter occupies larger area at higher injection pressure (Figure 16). Due to a better fuel spray penetration by the higher momentum at high injection pressure the fuel spray impinges to the chamber wall faster. In this case, the turbulence created close to the tip of the fuel spray and the improved mixing of liquidized and vaporized fuel with air promote the spatial ''expansion'' of the particulate matter.

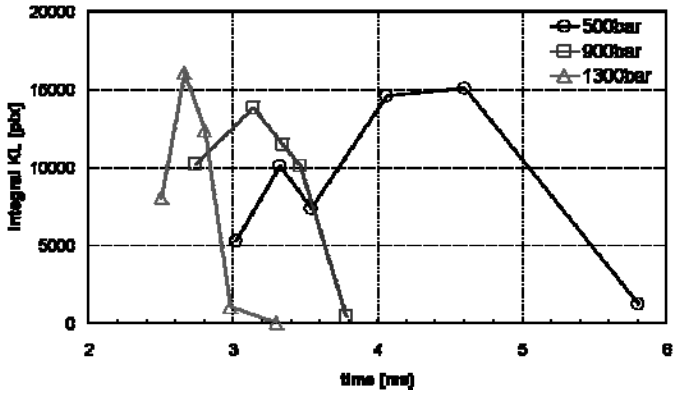

Figure 15: The integral of the KL-factor(sum of the KL-factor of the flame cross section) versus the time after the start of injection, at injection pressure 500bar, 900bar, 1300bar , keeping the injected diesel fuel mass constant

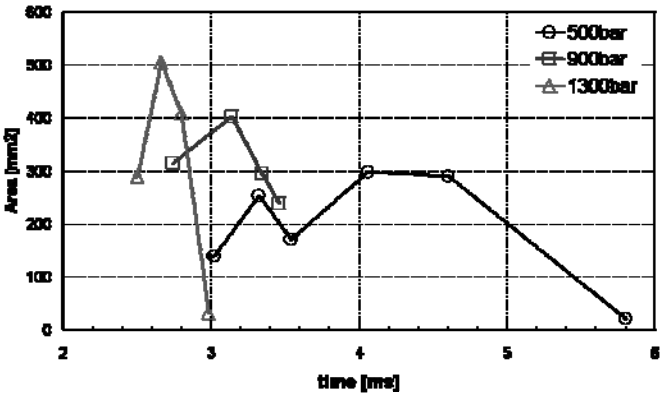

Figure 16: The surface of the particulate matter versus the time after the start of injection, at 500bar, 900bar, 1300bar, keeping the injected diesel fuel mass constant

Assuming that the fuel spray, in this experimental chamber, burns axisymetrically, the geometrical optical thickness L of the flame can be calculated qualitatively. The light intensity image serves as the base for the calculation of L. In Figure 17, the image is divided into vertical lines of 1 pixel width each (red lines). A secession of pixels with a nonzero value forms a line which represents a vertical slice through an imaginary axisymetric body (= circle). The first and the last pixels of this line have a geometrical optical thickness of zero; the pixel in the middle of these two pixels has the maximum optical thickness equal to the length of this line. This process is repeated for all vertical slices from left to right, which results in a 2D optical thickness distribution.

Applying the geometrical optical thickness and the KL-factor pixel-wise to equation

$$f_v = \frac{\lambda}{6\pi L \,\mathrm{Im}\left(\frac{m^2-1}{m^2+2}\right)} \cdot \frac{\kappa L}{\lambda^{\alpha}} \qquad (2)$$

the mean soot volume fraction (produced by burning diesel at different injection pressures) can be derived as shown in *Figure 18.*. Studying the development of the soot volume fraction at different injection pressures versus the time after start of the injection, it is observed that the peak values indicate the location where the total soot formation and the total soot oxidation across the cross-section of flame balance each other [9]. It is seen that the oxidation rate is higher at higher injection pressures. At high injection pres-

sures the fuel droplet size becomes smaller, thus the momentum transfer between the liquid phase and the gas phase increases, improving the mixing of both phases. Enhanced mixing quality results in the increase of the local oxygen contain, therefore the oxidation of the soot particles is improved.

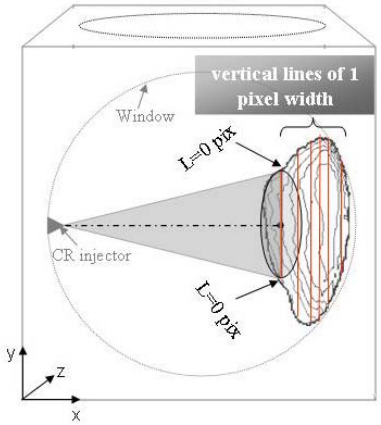

Figure 17: Schematic representation of combustion chamber, the fuel spray and the calculation of the flame optical thickness, based on the luminosity flame image

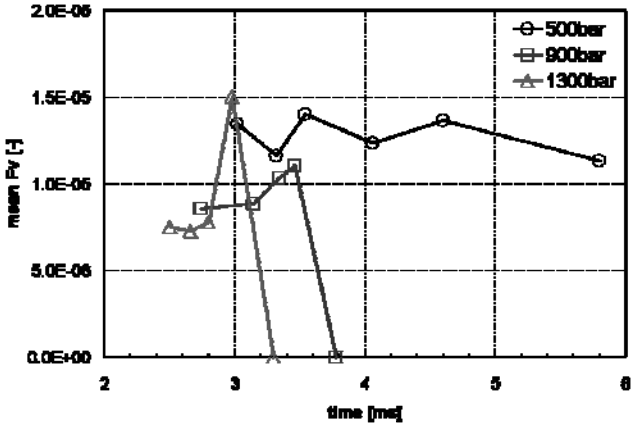

Figure 18: Evolution of the soot volume fraction versus the time after the start of the injection, at 500bar, 900bar and 1300bar, keeping the injected diesel fuel mass constant

Influence of Fuel Composition on the Emissions

Once the effects of the different injection pressure have been discussed, the influence of the different fuel composition on the emissions can be presented.

Five different fuels (baseline diesel fuel, two water-diesel emulsions containing 13% and 25% of water by mass respectively and two blends of 25% and 50% of oxygenated diesel fuel additive (butylal)) were considered in the present work. The properties of these fuels are given in the Table 2. To ensure a consistent comparison of the fuels, the temperature and the pressure of the cell were held constant at 790K and 60bar, respectively. The injection pressure was 500bar and the duration of injection for each fuel adjusted to account for the different lower heating values of the fuels; the different durations insured that the injected energy content was constant.

Fuel Type / Fuel Properties	Butylal	Diesel	25% Butylal Blend	50% Butylal Blend	13% W-D emulsion	25% W-D emulsion
Lower heating Value [MJ/kg]	35	43.14	41.11	39.07	37.98	34.27
Density at 15 C [kg/m^3]	834	828.5	822.7	826.5	850.6	866.5
Stoichiometric air/fuel ratio [kg/kg]	11.2	14.64	13.78	14.21	12.65	10.90
Water content [%]	0	-	25	50	12.89	22.16
Oxygen content [%]	19.97	0	4..99	9.99	11.24	18.8
Carbon [%]	67.45	86.08	81.42	76.77	75.1	67.77
Hydrogen [%]	12.58	13.89	13.56	13.24	13.66	13.43
Sulphur [ppm]	0	9.5	7.125	4.75	32.3	24.7
Kin. Viscosity at 40 C [mm2/s]	1.1	2.329	2.02	1.71	3.485	4.885
Cetane number [-]	74	51.4	-	-	-	-

Table 2: Characteristics of tested fuel tested in the present work; abbreviations W: water, D: diesel fuel

It has been observed that using the two blends of 25% and 50% of oxygenated diesel fuel additive (butylal) the mixing-controlled portion of the combustion is longer compared to the other fuels, while the premixed phase is the shortest (*Anhang Table 3-7*). It would be expected that these fuels produce higher quantities of soot, but Figures 20 and 21 show the opposite compared to diesel fuel. The flame temperature in these cases is quit high (Figure 22), meaning that the oxidation rate of the particulate matter decreases, while the O_2 concentration in the fuel makes the combustion leaner, acting in the opposite way; producing less soot.

The use of Water-Diesel emulsions has shown that during combustion their premixed phase is longer compared to the other fuels (*Anhang Table 3-7*). This possibly increases the NO_x emissions. On the other hand, the water evaporation lowers the post flame combustion temperature that is responsible for the NO_x emissions. In Figures 20 and 21 the low mean KL-factor obtained using water-diesel emulsions is presented. [10] has shown that increasing the quantity of water in the emulsions the mixing is improved because of the secondary atomization of the water droplets, leading to leaner combustion and so to lower KL-factor. Moreover, the controlled-mixing combustion is shorter compared to diesel and the blends of oxygenated diesel fuel additive. In this case the soot formation rate decreases. At the same time the oxidation rate decreases, because the flame temperature (Figure 22) is very low.

Looking at the oxygen content of the oxygenated blends and the emulsified fuels (Table 2), it can be observed that butylal 50% and the emulsion 13% contain almost the same percentage by mass of oxygen (respectively 9.99% and 11.24%) and carbon (respectively 76.77% and 75.1%). However, the peak of the mean KL-factor is found to be lower by the emulsion 13% at 500 bar injection pressure, while its integral is the same. Both compounds act as a source of oxygen, but in different ways: by butylal ($C_9H_{20}O_2$) the oxygen atom is bounded to two carbon atoms, while by the emulsion the oxygen is bounded to two hydrogen atoms, forming water. The dissociation energy of the C-O bond is lower than that of the H-O

[11], so oxygen gets free easier by butylal than by the emulsion. Nevertheless, the dissociation of water yields OH radicals [12], which are more effective in attacking soot precursors than single atoms or molecules of oxygen O and O_2 [13], released from the dissociation of butylal. The results show that at 500 bar injection pressure, the premixed phase duration is longer by the emulsion 13% than by butylal 50%, so that the mean KL-factor of the emulsion is lower.

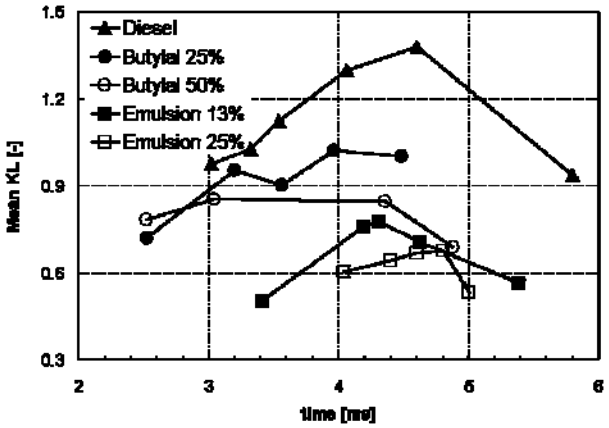

Figure 20: *The mean KL-factor for five fuels: diesel, 25% butylal-diesel blend, 50% butylal-diesel blend, 13% water-diesel emulsion and 25% water-diesel emulsion at 790K and 500bar*

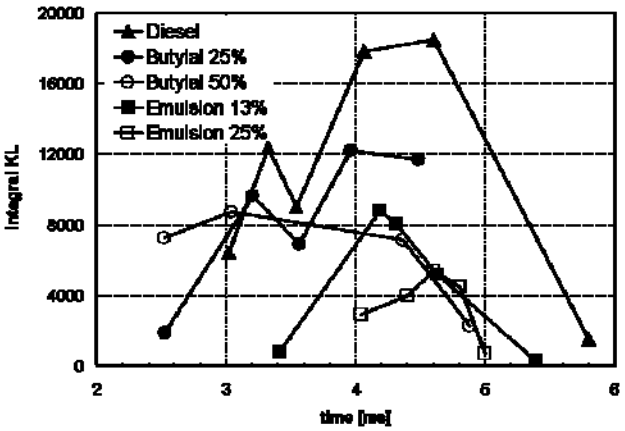

Figure 21: *The integral KL-factor for five fuels: diesel, 25% butylal-diesel blend, 50% butylal-diesel blend, 13% water-diesel emulsion and 25% water-diesel emulsion at 790K and 500bar*

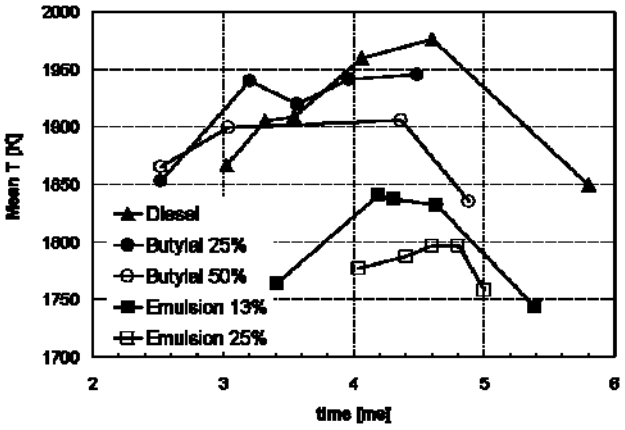

Figure 22: *The mean temperature for five fuels: diesel, 25% butylal-diesel blend, 50% butylal-diesel blend, 13% water-diesel emulsion and 25% water-diesel emulsion at 790K and 500bar*

Nationale Zusammenarbeit

We have an intensive and fruitful collaboration with the Reaction analysis Group (Dr. T. Dreier et.al.) of the Paul Scherrer Institute (PSI) on spray combustion research using both identical facilities (HTDZ) of the two institutions.

Internationale Zusammenarbeit

Collaboration on "Spray data base" proposed by ETH and PSI in the frame of the IEA implementing agreement "Energy conservation and emissions reduction in combustion" on the occasion of the 2003 Task Leaders meeting.

Schlussfolgerungen – Bewertung und Ausblick

Pyrometry and BDL technique are used for the investigation of soot formation and oxidation during combustion. The comparison of the two techniques showed that the mean KL-factor and its integral follow the same trend. However, the KL values calculated with BDL are rather lower compared to the pyrometer results. Further improvement of BDL technique is required.

Study of the influence of the injection pressure increase on the soot emissions and the flame temperature was conducted. Pyrometry measurements showed that injection pressure increase causes particulate matter and temperature decrease. Based on the temperature decrease, it can be concluded that the NOx emissions decrease.

Moreover, different fuels have been investigated by applying constant injection pressure (500bar) and constant fuel energy, in order to provide a detailed characterization of the influence of the fuel composition on combustion and emissions. Pyrometer results have shown that the mean temperature of the soot cloud decreases as a function of the fuel in the following order: diesel, butylal-diesel 25%, butylal-diesel 50%, water-diesel emulsions 13% and 25%. Both the mean KL-factor and its integral show the same trend.

These results are going to be used to complement the spray and combustion data for the validation of soot formation and oxidation models used in diesel engine combustion modeling. Publications based on the material of this year are prepared and are expected to be available in 2007. One doctoral dissertation on advanced turbulent combustion models (Y.M. Wright) has already used a set of these data for validation quite successfully. A second doctoral dissertation is at the final stage (examination planned for April 2007).

Referenzen

[1]* **Wright, Y.**: Numerical investigattion of turbulent spray combustion with conditional moment closure. Dissertation at Aerothermochemistry and Combustion Systems Laboratory at ETH Zurich: Diss. ETH Nr. 16386, Zurich, 2005.

[2] **Hirosho Tajima, Koji Takasaki**: Visual study on combustion of Low-Grade fuel water emulsion.

[3] **Heywood John B.**: Internal Combustion Engine Fundamentals. McGraw-Hill, 1988.

[4] **Zhao, H., Ladommatos, N.**: Optical diagnostics for soot and temperature measurement in Diesel engines. Prog. Energy Combust. Sci., Vol. 24, 1998.

[5]* **Kunte, S.**: Untersuchungen zum Einfluss von Brennstoffstruktur und -sauerstoffgehalt auf die Russbildung und -oxidation in laminaren Diffusionsflammen. Dissertation at Laboratorium für Verbrennungsmotoren und Verbrennungstechnik (LVV) at ETH Zürich: Diss. ETH Nr. 15003, Zürich, 2003.

[6]* **Raffael A. Schubiger**: Untersuchung zur Russbildung und –oxidation in der dieselmotorischen Verbrennung: Thermodynamische Kenngrössen, Verbrennungsanalyse und Mehrfarbenendoskopie. Dissertation at Laboratorium für Verbrennungsmotoren und Verbrennungstechnik (LVV) at ETH Zürich: Diss. ETH Nr. 14445, Zürich, 2001.

[7]* **O. Margari, S. Kunte, K. Boulouchos**: Particulate matter formation of Diesel fuel in a constant volume chamber, 9th Nanoparticle conference, ETH August 2005.

[8]* **K. Boulouchos, O. Margari, A. Escher, G. Barroso, B. Schneider, S. Kunte**: Optical Diagnostic on Diesel Sprays for the Validation of Computer Aided Simulation, 6. Internationales Symposium für Verbrennungsdiagnostik, AVL June 2004.

[9] **Pickett L.M., Siebers D.L.**: "Soot in diesel fuel jets: effects of ambient temperature, ambient density, and injection pressure", Combustion and Flame, Vol. 138, pp. 114-135, 2004.

[10] **Kosaka H., Aizawa T., Kamimoto T.**: Two-dimensional imaging of ignition and soot formation proesses in a diesel flame, 2 August 2004.

[11]* **Bertola, A**.: Technologies for Lowest NO_x and Particulate Matter Emissions in DI-Diesel Engine Coimbustion-Influence of Injection Parameters, EGR and Fuel Composition, Diss ETH No. 15373, 2003.

[12] **C.E. Mortimer, U. Müller**: "Chemie - Das Basiswissen der Chemie", 8. Auflage, Georg Thieme Verlag, Stuttgart, 2003.

[13] **O. Armas, R. Ballesteros, F.J. Martos, J.R. Agudelo**: "Characterization of light duty Diesel engine pollutant emissions using water-emulsified fuel", Fuel, Vol. 84, pp. 1011-1018, 2005.

[14] **K.G. Neoh, J.B. Howard, A.F. Sarofim**: "Soot Oxidation in Flames", In: D.C. Siegla, G.W. Smith, "Particulate Carbon: Formation During Combustion", pp. 261-277, Plenum Press, New York, (1981).

[15]* **Margari, O.**: Experimental investigation of transient sprays with combustion, Dissertation at Aerothermochemistry and Combustion Systems Laboratory at ETH Zurich, planned for April 2007.

*Publications marked with a * are our own ones.*

Anhang

DIESEL	Ignition Delay	Premixed Combustion	Diffusion Combustion	Combustion Duration
p_{inj} [bar]	[ms]	[ms]	[ms]	[ms]
500	2.25	0.55	3.55	4.10
900	1.70	0.80	2.20	3.00
1300	1.40	0.95	1.60	2.55

Table 3: Diesel: combustion characteristics

BUTYLAL 25%	Ignition Delay	Premixed Combustion	Diffusion Combustion	Combustion Duration
p_{inj} [bar]	[ms]	[ms]	[ms]	[ms]
500	1.45	0.50	4.35	4.85
900	1.40	0.55	2.85	3.40
1300	1.10	0.75	1.65	2.40

Table 4: Dlend diesel-butylal 25%: combustion characteristics

BUTYLAL 50%	Ignition Delay	Premixed Combustion	Diffusion Combustion	Combustion Duration
p_{inj} [bar]	[ms]	[ms]	[ms]	[ms]
500	1.70	0.30	4.15	4.45
900	1.35	0.52	2.85	3.37
1300	1.35	0.45	2.20	2.65

Table 5: Dlend diesel-butylal 50%: combustion characteristics

W-D 13%	Ignition Delay	Premixed Combustion	Diffusion Combustion	Combustion Duration
p_{inj} [bar]	[ms]	[ms]	[ms]	[ms]
500	2.15	0.77	2.85	3.62
900	1.90	0.45	1.82	2.27
1300	-	-	-	-

Table 6: Water-Diesel emulsion 13%: combustion characteristics

W-D 25%	Ignition Delay	Premixed Combustion	Diffusion Combustion	Combustion Duration
p_{inj} [bar]	[ms]	[ms]	[ms]	[ms]
500	1.62	1.30	2.85	4.15
900	1.42	1.18	1.82	3.00
1300	-	-	-	-

Table 7: Water-Diesel emulsion 25%: combustion characteristics